Recombination velocity less than 100 cm/s at polycrystalline Al₂O₃/CdSeTe interfaces

Cite as: Appl. Phys. Lett. **112**, 263901 (2018); https://doi.org/10.1063/1.5030870 Submitted: 26 March 2018 . Accepted: 15 June 2018 . Published Online: 27 June 2018

Darius Kuciauskas 📵, Jason M. Kephart 📵, John Moseley, Wyatt K. Metzger, Walajabad S. Sampath, and Pat Dippo







ARTICLES YOU MAY BE INTERESTED IN

The roles of carrier concentration and interface, bulk, and grain-boundary recombination for 25% efficient CdTe solar cells

Journal of Applied Physics 121, 214506 (2017); https://doi.org/10.1063/1.4984320

Emitter/absorber interface of CdTe solar cells

Journal of Applied Physics 119, 233104 (2016); https://doi.org/10.1063/1.4953820

CdCl₂ passivation of polycrystalline CdMgTe and CdZnTe absorbers for tandem photovoltaic cells

Journal of Applied Physics 123, 203101 (2018); https://doi.org/10.1063/1.5023811







Recombination velocity less than 100 cm/s at polycrystalline Al₂O₃/CdSeTe interfaces

Darius Kuciauskas,^{1,a)} Jason M. Kephart,^{2,b)} John Moseley,¹ Wyatt K. Metzger,¹ Walajabad S. Sampath,² and Pat Dippo¹

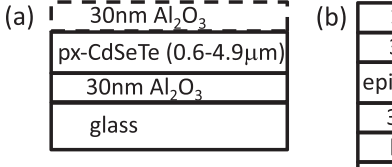
¹National Renewable Energy Laboratory, 15013 Denver West Parkway, Golden, Colorado 80401, USA ²Department of Mechanical Engineering, Colorado State University, Fort Collins, Colorado 80523, USA

(Received 26 March 2018; accepted 15 June 2018; published online 27 June 2018)

Reducing recombination in polycrystalline solar cells by orders of magnitude is currently one of the greatest challenges for increasing thin-film solar cell efficiency to theoretical limits. The question of how to do this has been a challenge for the thin-film community for decades. This work indicates that effective interface passivation is critical. Here, polycrystalline Al₂O₃/CdSeTe/Al₂O₃/glass heterostructures are grown, and a combination of spectroscopic, microscopic, and time-resolved electro-optical measurements demonstrates that the interface recombination velocity at alumina/thin-film interfaces can be less than 100 cm/s. This is three orders of magnitude less than typical CdTe interfaces without passivation, commensurate with single-crystal epitaxial CdMgSeTe/CdSeTe/CdMgSeTe double heterostructures, and enables minority-carrier lifetimes in polycrystalline CdSeTe well above 100 ns. Microscopic interfacial electric-field measurements identify the field effect as a potential mechanism for polycrystalline Al₂O₃/CdSeTe interface passivation. The results provide guidance for modeling and interface passivation in devices and indicate future paths to realize highly efficient thin-film solar cells. *Published by AIP Publishing*. https://doi.org/10.1063/1.5030870

Thin-film solar cell technologies are a promising approach to realize highly efficient and low-cost photovoltaics (PV) to provide electricity at lower costs than fossil fuels. However, as thin-film absorbers are just several microns thick and crystalline grains are on the order of microns, both the grain boundary and interface recombination can significantly limit voltage, and hence, they can limit these technologies from attaining higher efficiency. Precisely, how to engineer longer carrier lifetimes in light of these challenges represents a key issue for thin-film PV.

Simulations indicate that for 25%-efficient thin-film solar cells based on carrier drift at the semiconductor pn junction, direct-bandgap absorbers need a minority-carrier lifetime (τ_B) of >100 ns, a hole density of >10¹⁶ cm⁻³, and an interface recombination velocity (S) of $\leq 1000 \,\mathrm{cm/s.}^1$ These characteristics were demonstrated in single-crystal and epitaxial CdTe, which enabled CdTe solar cells with an open-circuit voltage of >1 V.^{2,3} Efforts are underway to achieve similar results with less expensive polycrystalline (px) thin films. A carrier concentration of $>10^{16} \text{ cm}^{-3}$ is enabled with group-V dopants.4 The minority-carrier lifetime is substantially improved with Se alloying in the absorber, 5,6 but the defect physics in CdSeTe remains unclear. Surface recombination velocities for as-grown single-crystal, epitaxial (epi), and px-CdTe are greater than 10⁵ cm/s, and passivation is needed to reduce interface recombination. A myriad of etches and anneals to reduce contaminants, remove oxides, adjust interfacial stoichiometry, and reconstruct polycrystalline and single-crystal Because of the importance of interface passivation, we report on the electro-optical (EO) properties of px-Al₂O₃/CdSeTe/Al₂O₃ double heterostructures (DHs) grown on glass substrates. A schematic of the structure is shown in Fig. 1(a). The Al₂O₃ layers are deposited by sputtering and the CdSeTe layers by close-spaced sublimation. The EO properties of polycrystalline CdTe and CdSeTe DHs are compared, and further growth details are given in Ref. 9. CdSe_xTe_{1-x} DHs studied here were grown from the source material with x = 0.2. Based on the bandgaps estimated with electronic spectroscopy (see Fig. 2) and published CdSe_xTe_{1-x} analysis, ¹⁵ $x \approx 0.15$ in polycrystalline samples in this study. We also compare px-DH



(b)	10nm CdTe
	30nm CdSeMgTe
	epi-CdSeTe (0.5-2μm)
	30nm CdSeMgTe
	buffer
	InSb(100)

surfaces has thus far not been sufficient to achieve $S < 10^4$ cm/s, although Cd-rich stoichiometry has significantly reduced recombination. To mitigate px-CdTe interfacial recombination, Kephart *et al.* applied sputter-deposited oxides and observed the best time-resolved photoluminescence (TRPL) lifetimes with alumina (Al₂O₃) and CdSeTe absorbers. Alumina was also applied to passivate the back contacts of CdTe solar cells 10-12 and to improve sample preparation for electron-beam-induced-current (EBIC) microscopy. 13,14

a)Darius.Kuciauskas@nrel.gov

b)Current address: First Solar, 1035 Walsh Ave., Santa Clara, California 95050, USA. Electronic mail: Jason.Kephart@firstsolar.com.

FIG. 1. Illustration of substrate, absorber, and passivation layers in polycrystalline (a, Ref. 9) and single-crystal epitaxial (b, Ref. 16) double heterostructures studied here.

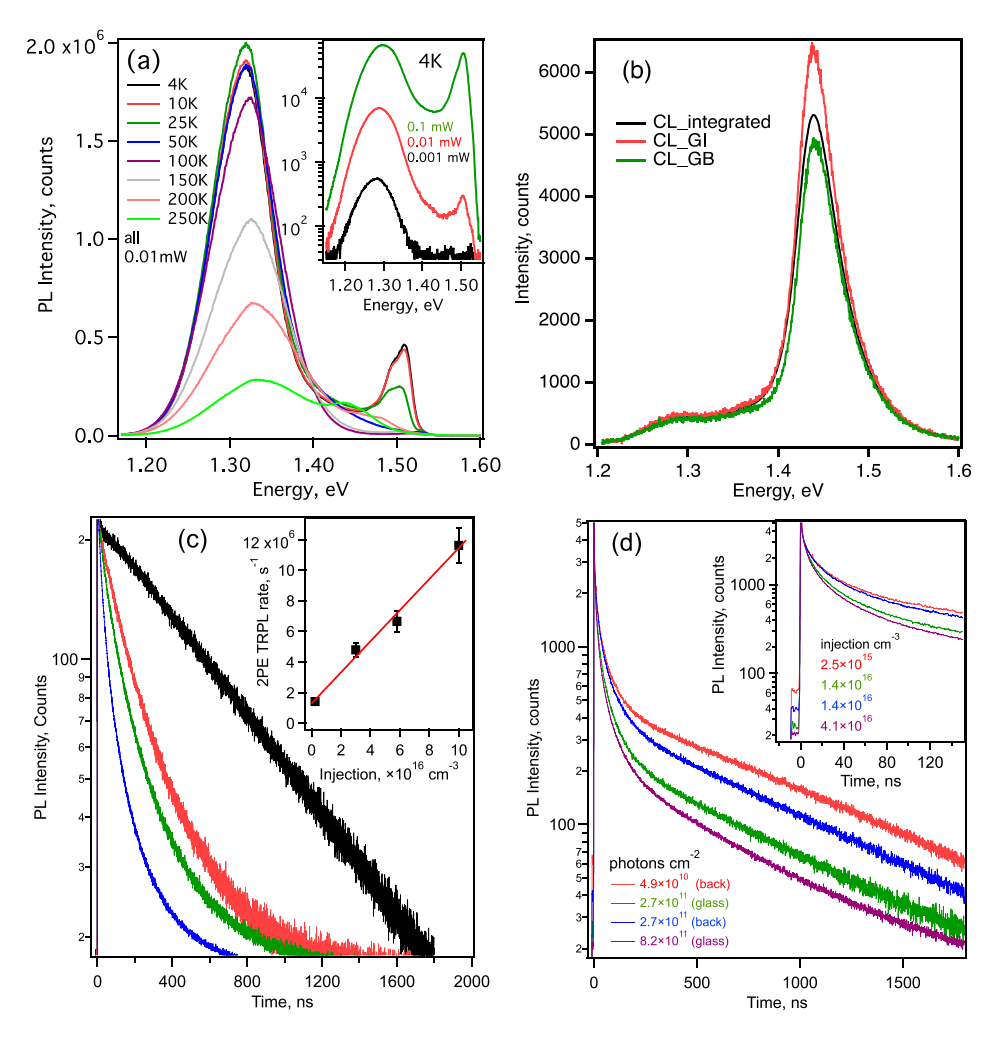


FIG. 2. (a) PL emission spectra at 4–250 K, (b) room-temperature CL spectra, (c) 2PE TRPL decays, and (d) 1PE TRPL decays for a px-DH with 2.5- μ m absorber thickness (DH3). The inset in (a) shows PL emission spectra at 4 K when the excitation power is 1, 10, and 100 μ W. Pixel locations for grain interior (GI) and grain boundary (GB) CL spectra in (b) are indicated in Fig. 3. The inset in (c) shows the 2PE TRPL decay rate dependence on injection. The inset in (d) shows 1PE TRPL dynamics on a faster time scale.

properties with previously reported EO characteristics for epi-CdSe $_x$ Te $_{1-x}$ DHs [see Fig. 1(b)] grown by molecular beam epitaxy (MBE), where x=0.008 was used to improve lattice matching to the substrate. Growth and characterization details for epi-DHs can be found in Ref. 16. Remarkably, although the px-DHs are grown by fast and low-cost manufacturable methods relevant to current CdTe solar cell technology, we find similarly low interface recombination velocity as for DHs grown with exquisite but expensive control by MBE.

We analyzed several px-DHs where the CdSeTe absorber thickness was varied from 0.6 to $4.9 \,\mu\text{m}$. We first present a detailed analysis for a px-DH where the absorber thickness is $2.5 \,\mu\text{m}$ (Figs. 2 and 3), then analyze carrier lifetimes when the absorber thickness is varied (Fig. 4), and

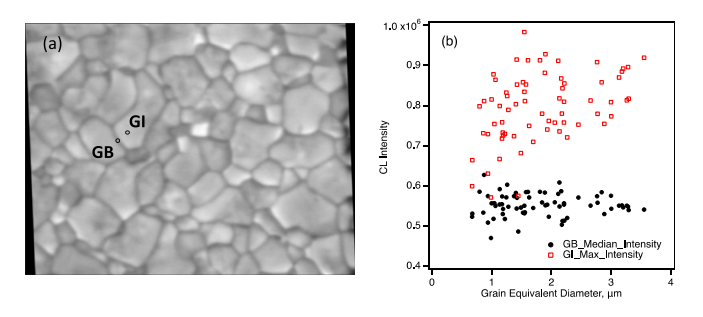


FIG. 3. (a) CL image for px-DH with a 2.5- μ m thick absorber. Labels GB and GI show pixel locations for which CL spectra are shown in Fig. 2(b). The field of view is $20.7 \times 15.8~\mu m^2$. (b) Distribution of GI maximal and GB median CL intensities for 69 grains identified in (a) by image processing.

finally examine interface passivation mechanisms in px- and epi-DHs (Fig. 5).

Several EO characterization techniques were applied. Time-resolved photoluminescence (TRPL) was measured with

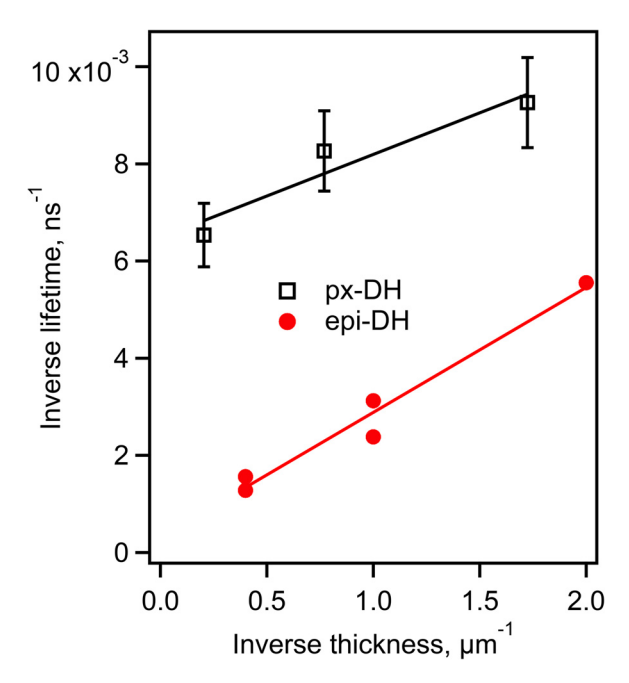


FIG. 4. 2PE TRPL decay rate (lifetime $^{-1}$) thickness dependence for px-Al₂O₃/CdSeTe/Al₂O₃ DHs (squares) and epi-CdSeMgTe/CdSeTe/CdSeMgTe DHs (circles, reproduced from Ref. 16).

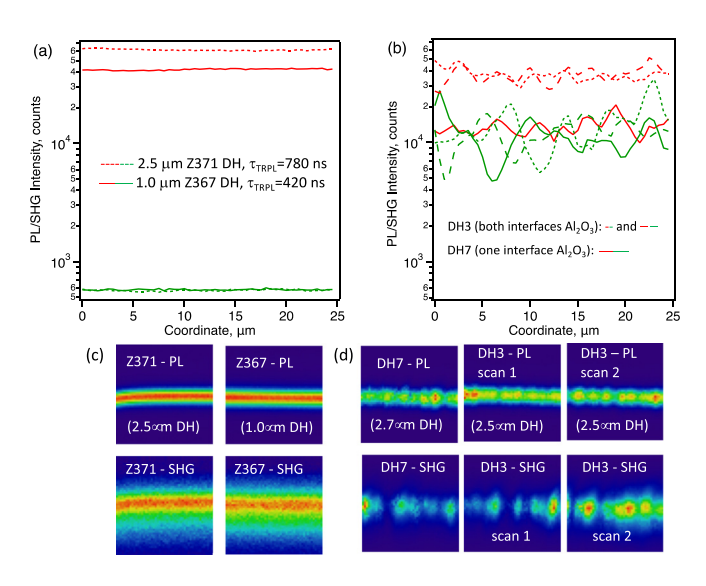


FIG. 5. Comparison of PL and SHG intensities for epi- (a and c) and px- (b and d) DHs. Absorbers in epi-DHs are $1.0\,\mu\mathrm{m}$ and $2.5\,\mu\mathrm{m}$ thick. Px-DHs have passivation at both (DH3, dashed lines) or one (DH7, solid lines) interfaces. Graphs show linear intensity profiles (single-photon counts measured every $0.5\,\mu\mathrm{m}$) for PL (red) and SHG (green). Images show normalized PL and SHG intensities in cross sections (the field of view is $25\times25\,\mu\mathrm{m}^2$). To illustrate that averaged PL and SHG intensities are reproducible for polycrystalline samples, two scans of different sample areas are shown for DH3. Sample structures are illustrated in Fig. 1.

unfocused excitation (0.3-mm excitation spot diameter) at 640 nm for one-photon excitation (1PE) and at 1120 nm for twophoton excitation (2PE). The former has been well correlated with device performance in polycrystalline devices and yields similar values for materials without contacts. 17-19 The TRPL technique also gives similar results to transient free-carrier absorption and microwave conductivity measurements.²⁰ 2PE photoluminescence (PL) and second-harmonic generation (SHG) microscopy data were measured with focused diffraction-limited excitation at 1030 nm. Variable-temperature PL emission spectra were measured by placing samples in a closed-loop He cryostat and exciting with a HeNe (632.8-nm) continuous-wave (cw) laser. Cathodoluminescence (CL) spectrum imaging was carried out at room temperature with a JEOL 7600F scanning electron microscope and a Horiba HCLUE CL system. The electron-beam conditions were 7.5-kV accelerating voltage and about 3-nA current. Surface preparation for CL included ion milling with an inert Ar⁺ ion beam at a glancing angle (\approx 5°) (JEOL Cross-Section Polisher). Computational modeling with Sentaurus was used to simulate the TRPL experiments on Al₂O₃/CdSeTe/Al₂O₃ double heterostructures of different thicknesses with columnar grain boundaries and variable inputs for the interface, grain boundary (GB), and bulk lifetime to verify self-consistency and aid interpretation.²¹

The CdCl₂ treatment typically improves the EO CdTe properties (as evaluated, for example, by the stronger PL emission intensity), and the CdCl₂ treatment was used in the px-DH samples studied here. The absorber layer and Al₂O₃ were nominally undoped (Cu treatment was not used), but the background doping in CdTe after CdCl₂ treatment is lightly ptype. The low-temperature bandgap (E_g) of \approx 1.53 eV is extrapolated from the excitonic features in the 4 K PL emission spectra [Fig. 2(a)]. At 300 K, E_g \approx 1.47 eV from the CL spectra [Fig. 2(b)]. These values are \approx 80 meV smaller relative

to E_g for CdTe due to Se alloying.²² The average CdSeTe crystalline grain size (Fig. 3) was $1.8 \pm 0.8 \mu m$.

The PL emission spectra [Fig. 2(a)] have broad emission lines attributed to bound excitons (1.51-eV maximum and 1.49-eV shoulder at 4–10 K) and to deep defects (1.32-eV maximum at 4–50 K). The broadening can be related to spectral heterogeneity, which can be created due to nonuniform Se compositions as observed in other CdSeTe absorbers by atom probe tomography (APT). Figure 2 also shows TRPL decays measured with 2PE (c) and 1PE (d). Because DHs are undoped, low carrier-injection ΔN is needed to determine minority-carrier lifetimes. As shown in (c), we observe single-exponential 2PE TRPL decays (lifetime $\tau_{\rm 2PE} = 700 \pm 70\,\rm ns$) when $\Delta N = 2 \times 10^{15}\,\rm cm^{-3}$. Recombination rates $\tau_{\rm 2PE}^{-1}$ are larger at higher ΔN . As shown in the inset of (c), the $\tau_{\rm 2PE}^{-1}$ dependence on ΔN can be analyzed as $\tau_{\rm 2PE}^{-1}$

$$\frac{1}{\tau_{2PE}} = \frac{1}{\tau_{SRH}} + B(\Delta N)\Delta N; B(\Delta N) = B_{rad}/(1 + \Delta N/N_b), \quad (1)$$

where τ_{SRH}^{-1} is the Shockley-Read-Hall (SRH) recombination rate (assumed to be equal to τ_{2PE}^{-1} at the lowest injection), B_{rad} is the radiative recombination coefficient at low injection, 25 and $N_b = 7 \times 10^{18} \, \mathrm{cm}^{-3}$ is the carrier density when injection-dependent $B(N_b)$ becomes two times smaller than B_{rad} . This model fits the data, which suggests that trapping does not significantly affect carrier lifetimes in px-DHs. DH-thickness-dependent TRPL lifetimes (shown in Fig. 4) also show that trapping is not significant in samples studied here.

1PE TRPL decays [Fig. 2(d)] have a faster initial decay component, even when the injection level is comparable to 2PE. Computational simulations indicate that this is caused by the difference in the carrier generation profiles. In 2PE generation, carriers are generated uniformly through the absorber thickness (2.5 μ m). On the other hand, in 1PE generation, about 50% and 90% of the carriers are generated within 0.12 μ m and 0.4 μ m from the interface in a Beer law distribution. This causes a fast transient in the luminescence as the electrons and holes diffuse into the bulk of the material. Importantly, the 1PE TRPL decays also have long-lifetime components $\tau_{1PE} = 560-770 \, \text{ns.}^9$ Therefore, both 1PE and 2PE data indicate the long bulk carrier lifetime.

Figure 3 shows a spectrally integrated CL microscopy image for the same px-DH3 (Al₂O₃/CdSeTe/Al₂O₃) where Al₂O₃ was removed by ion milling for (a) CL microscopy and (b) the statistical analysis of the grain interior (GI)/grain boundary (GB) CL intensity distribution.²⁶ GB defects can cause recombination and shift the Fermi level, generally in such a way that minority carrier attractive GB potentials are formed.^{27–30} In px-CdTe, these GB potentials are generally on the order of tens of mV,³¹ and injected carriers from the electron beam will screen these fields and reduce their effect on charge separation.²¹ Modeling to be presented in future work³² indicates that a minor amount of CL decrease occurs due to the field near the GB core, but the majority of CL intensity drop across the GBs is caused by recombination.

For statistical analysis, CL intensity can be described by the GI/GB contrast. When the grain equivalent diameter is $\geq 2 \, \mu \text{m}$, the GI/GB contrast in the CL data, defined as (GI_Max_Intensity – GB_Median_Intensity)/GI_Max_Intensity,

is about constant at 0.32 ± 0.05 , which is lower than such contrast for px-CdTe studies, ³⁴ and suggests lower GB recombination in CdSeTe. Because ion milling was used to prepare the CdSeTe surface for CL analysis and this treatment changes the interface, the CL data are distinct from the original DH and not used to quantify recombination.

Next, we analyze interface recombination from the TRPL lifetimes measured for DHs that differ in the absorber thickness ($d = 0.6, 1.3, \text{ and } 4.9 \, \mu\text{m}$) using³⁵

$$\frac{1}{\tau_{TRPL}} = \frac{1}{\tau_B} + \frac{2S}{d},\tag{2}$$

where τ_{TRPL} is the measured lifetime for a DH with absorber thickness d. This model requires uniform generation in the absorber; 35 therefore, we used 2PE to ensure uniform generation and to obtain low injection. The fit with Eq. (2) to the px-DH TRPL lifetimes in Fig. 4 gives $\tau_{B,px} = 154 \pm 14 \, \text{ns}$ and $S_{\text{DX}} = 85 \pm 25 \, \text{cm/s}.$

DHs are commonly used to analyze the EO properties of epitaxial heterostructues. 3,16,35 When analyzing epi-CdTe and epi-CdSeTe DHs together, Zaunbrecher *et al.* reported $S_{\rm epi}=160\,{\rm cm/s}$ and $\tau_{\rm B,epi}=2.2~\mu{\rm s.}^{16}$ We reproduce epi-CdSeTe data from the study by Zaunbrecher *et al.* in Fig. 4 (red circles), where the fit shows slightly improved characteristics for the epi-CdSeTe DHs with $S_{\rm epi}=125\pm15\,{\rm cm/s}$ and $\tau_{\rm B,epi}=3.2\pm0.3~\mu{\rm s.}$

Shorter carrier lifetimes in px-DHs ($\tau_{B,px} = 154 \pm 14 \, \text{ns}$ vs. $\tau_{\rm B.epi} = 3.2 \pm 0.3 \ \mu \rm s$) relative to epitaxial material can be attributed to SRH recombination due to bulk and GB defects. At the same time, a carrier lifetime of $\tau_{B,px} = 154 \, \text{ns}$ is very high for polycrystalline absorbers. 6,17,19,36 Inserting the median grain size of $2 \mu m$ from the CL measurements into the computational DH model indicates that the GB recombination velocity here is less than 10^3 cm/s. This is consistent with the low CL GI/GB contrast (Fig. 3) and 1PE/2PE TRPL lifetimes >100 ns (Figs. 2 and 4). Interestingly, although the GB recombination velocity is low, it is likely the leading source of recombination in the high quality px-DHs. To develop polycrystalline absorbers where $\tau_{\rm B}$ is limited by radiative recombination, it will be important to understand CdSeTe GB and bulk defect properties. For example, the population and properties of SRH recombination centers, such as Te_{Cd} antisite, ^{37,38} can be different in CdTe vs. CdSeTe and in epi- vs. px-absorbers.

In contrast to different τ_B values, the interface recombination velocities are comparable in the epi- and px-DHs, $S_{epi}=125\pm15$ cm/s and $S_{px}=85\pm25$ cm/s. To translate these encouraging results to device applications, it is important to examine the potential passivation mechanisms. In principle, both field-effect and defect passivation could reduce interface recombination, but such passivation mechanisms could have different effects on devices. The passivation mechanism at $Al_2O_3/CdSeTe$ interfaces is not understood. $^{9-11,13,14}$ To probe passivation at epi- and px-interfaces, we used SHG microscopy. As-grown CdTe surfaces have been reported to be positively charged, which leads to electrostatic band bending. 7,10,39 Such an electrostatic near-interface space-charge field (SCF) can be analyzed using optical SHG measurements.

CdTe⁴³ and px-CdTe⁴⁴ interfaces, the SHG optical signal has been observed due to electric field induced second harmonics (EFISH). With SHG/EFISH microscopy, it is possible to analyze lateral SCF distributions. For defect passivation, the SCF strength is expected to be reduced, which will be observed as a lower EFISH intensity. For the field-effect passivation, a more complex charge distribution is observed, for example, at Al₂O₃/Si^{40,41,45} and ITO/a-Si:H⁴² interfaces.

Figure 5 compares PL and SHG intensities for (a and c) two epi- and (b and d) two px-DHs when the same excitation conditions and measurement optics were used. In epitaxial samples, PL and SHG intensities are spatially uniform, and the SHG intensity is weaker than that of PL by a factor of about 100. In the px samples, the SHG intensity is comparable to the PL intensity. Comparison of SHG intensity in (a) and (b) show that SHG is about 23x stronger for px-DHs than for epi-DHs. Because the EFISH intensity is proportional to the square of the electric field, 46 the SCF is \approx 4.8x ($\sqrt{23}$ x) stronger at px interfaces. These data are consistent with the epi- and px- interfaces studied here having defect passivation and field-effect passivation, respectively.

In Figs. 5(b) and 5(d), we compare the PL and SHG intensities for a CdSeTe/Al₂O₃/glass absorber (DH7) where the "top" of the CdSeTe absorber was not passivated and an Al₂O₃/CdSeTe/Al₂O₃/glass absorber (DH3) where alumina was applied to both interfaces. The PL intensity increases for DH3, which is attributed to passivation at both interfaces. In contrast, the SHG intensity is about the same for DH3 and DH7. Comparable EFISH intensities for DH3 and DH7 imply that the SCF strength is similar for the CdSeTe and Al₂O₃/CdSeTe samples.⁴⁷

Additional studies are needed to understand charge distribution at the Al₂O₃/CdSeTe interfaces. EFISH microscopy has sufficient resolution to observe lateral SCF variations between the grains, but the axial (vertical) resolution in optical SHG/EFISH measurements is only ≈100 nm (estimated as $1/\alpha_{515\,\mathrm{nm}}$, where $\alpha_{515\,\mathrm{nm}}$ is the absorption coefficient at the SHG wavelength⁴⁸). Therefore, if several charged layers are present at the interface (such as, for example, positively charged CdTe³⁹ and negatively charged Al₂O₃⁴⁵), they will not be resolved in optical measurements. It is most likely that EFISH probes the electric field in the CdSeTe spacecharge region (but not the interface dipoles or other interface charges), as is the case for Al₂O₃/Si^{40,41} and ITO/a-Si:H.⁴² This is because the EFISH intensity does not change with and without the top Al₂O₃ layer in px-DHs and also because the EFISH intensity correlates with the minority-carrier dynamics near the extended defects in epi-DHs. 43 The minority-carrier dynamics indirectly suggest that nearinterface barriers prevent electron recombination at px-Al₂O₃/CdSeTe interfaces. This is seen in 2PE TRPL data [Fig. 2(c)], where at the lowest injection, we observe only the long-lifetime component of the PL decay. Because 2PE TRPL data in Fig. 2 are averaged over the large area (diameter $\approx 300 \,\mu\text{m}$), the barrier appears to be effective despite the lateral SCF strength variation (Fig. 5).

In conclusion, we have shown that interface recombination is reduced to $S_{px} < 100\,\text{cm/s}$ for px-Al $_2$ O $_3$ /CdSeTe interfaces. SHG measurements indicate that this can be

consistent with field-effect passivation. Furthermore, the GB recombination velocity is small. This enables lifetimes of hundreds of ns in low-cost, high-deposition-rate polycrystal-line solar cell absorbers that are compatible with industrial fabrication processes. Additional theoretical, modeling, and experimental studies are required to understand CdSeTe bulk, surface, and GB defect properties. The results also show that px-DHs are useful model systems for the EO analysis of polycrystalline thin films, and they provide research paths to better understand, and perhaps further increase, the performance of thin-film solar cells.

We thank Thomas H. Myers (Texas State University) for epitaxial double heterostructures. J.K. would like to thank Amit Munshi for his help with CdSeTe deposition. This work was funded by the U.S. Department of Energy's Office of Energy Efficiency and Renewable Energy (EERE) under Solar Energy Technologies Office (SETO) Agreement Nos. 30306, 30307, and DE-EE0007365. At NREL, this work was supported by the U.S. Department of Energy under Contract No. DE-AC36-08-GO28308 with the National Renewable Energy Laboratory. The U.S. Government retains, and the publisher, by accepting the article for publication, acknowledges that the U.S. Government retains a nonexclusive, paid up, irrevocable, worldwide license to publish or reproduce the published form of this work, or allow others to do so, for U.S. Government purposes.

- ¹A. Kanevce, M. O. Reese, T. M. Barnes, S. A. Jensen, and W. K. Metzger, J. Appl. Phys. **121**, 214506 (2017).
- ²J. M. Burst, J. N. Duenow, D. S. Albin, E. Colegrove, M. O. Reese, J. A. Aguiar, C.-S. Jiang, M. K. Patel, M. M. Al-Jassim, D. Kuciauskas, S. Swain, T. Ablekim, K. G. Lynn, and W. K. Metzger, Nat. Energy 1, 16015 (2016).
- ³Y. Zhao, M. Boccard, S. Liu, J. Becker, X.-H. Zhao, C. M. Campbell, E. Suarez, M. B. Lassise, Z. Holman, and Y.-H. Zhang, Nat. Energy 1, 16067 (2016).
- ⁴S. Grover, X. Li, W. Zhang, M. Yu, G. Xiong, M. Gloeckler, and R. Malik, in 2017 IEEE 44nd Photovoltaic Specialists Conference (IEEE, 2017)
- ⁵A. H. Munshi, J. Kephart, A. Abbas, J. Raguse, J. Beaudry, K. Barth, J. Sites, J. Walls, and W. Sampath, IEEE J. Photovoltaics **8**, 310 (2018).
- ⁶M. Amarasinghe, E. Colegrove, J. Moseley, H. Moutinho, D. Albin, J. Duenow, S. Jensen, J. Kephart, W. Sampath, S. Sivananthan, M. Al-Jassim, and W. K. Metzger, Adv. Energy Mater. 8, 1702666 (2018).
- ⁷M. O. Reese, C. L. Perkins, J. M. Burst, S. Farrell, T. M. Barnes, S. W. Johnston, D. Kuciauskas, T. A. Gessert, and W. K. Metzger, J. Appl. Phys. 118, 155305 (2015).
- ⁸M. O. Reese, J. M. Burst, C. L. Perkins, A. Kanevce, S. W. Johnston, D. Kuciauskas, T. M. Barnes, and W. K. Metzger, IEEE J. Photovoltaics 5, 382 (2015).
- ⁹J. M. Kephart, A. Kindvall, D. Williams, D. Kuciauskas, P. Dippo, A. Munshi, and W. S. Sampath, IEEE J. Photovoltaics **8**, 587 (2018).
- ¹⁰J. Liang, Q. Lin, H. Li, Y. Su, X. Yang, Z. Wu, J. Zheng, X. Wang, Y. Lin, and F. Pan, Appl. Phys. Lett. **107**, 13907 (2015).
- ¹¹Y. Su, C. Xin, Y. Feng, Q. Lin, X. Wang, J. Liang, J. Zheng, Y. Lin, and F. Pan, ACS Appl. Mater. Interfaces 8, 28143 (2016).
- ¹²Q. Lin, Y. Su, M.-J. Zhang, X. Yang, S. Yuan, J. Hu, Y. Lin, J. Liang, and F. Pan, Chem. Commun. **52**, 10708 (2016).
- ¹³B. Bissig, C. Guerra-Nunez, R. Carron, S. Nishiwaki, F. La Mattina, F. Pianezzi, P. A. Losio, E. Avancini, P. Reinhard, S. G. Haass, M. Lingg, T. Feurer, I. Utke, S. Buecheler, and A. N. Tiwari, Small 12, 5339 (2016).
- ¹⁴B. Bissig, M. Lingg, C. Guerra-Nunez, R. Carron, F. La Mattina, I. Utke, S. Buecheler, and A. N. Tiwari, Thin Solid Films 633, 218 (2017).
- ¹⁵G. Brill, Y. Chen, P. M. Amirtharaj, W. Sarney, D. Chandler-Horowitz, and N. K. Dhar, J. Electron. Mater. 34, 655 (2005).

- ¹⁶K. N. Zaunbrecher, D. Kuciauskas, C. H. Swartz, P. Dippo, M. Edirisooriya, O. S. Ogedengbe, S. Sohal, B. L. Hancock, E. G. LeBlanc, P. A. R. D. Jayathilaka, T. M. Barnes, and T. H. Myers, Appl. Phys. Lett. 109, 91904 (2016).
- ¹⁷W. K. Metzger, D. Albin, D. Levi, P. Sheldon, X. Li, B. M. Keyes, and R. K. Ahrenkiel, J. Appl. Phys. **94**, 3549 (2003).
- ¹⁸W. K. Metzger, D. Albin, M. J. Romero, P. Dippo, and M. Young, J. Appl. Phys. **99**, 103703 (2006).
- ¹⁹D. Kuciauskas, P. Dippo, Z. Zhao, L. Cheng, A. Kanevce, W. K. Metzger, and M. Gloeckler, IEEE J. Photovoltaics 6, 313 (2016).
- ²⁰S. Johnston, K. Zaunbrecher, R. Ahrenkiel, D. Kuciauskas, D. Albin, and W. Metzger, IEEE J. Photovoltaics 4, 1295 (2014).
- ²¹W. K. Metzger, R. K. Ahrenkiel, J. Dashdorj, and D. J. Friedman, Phys. Rev. B 71, 035301 (2005).
- ²²N. R. Paudel and Y. Yan, Appl. Phys. Lett. **105**, 183510 (2014).
- ²³J. D. Poplawsky, W. Guo, N. Paudel, A. Ng, K. More, D. Leonard, and Y. Yan, Nat. Commun. 7, 12537 (2016).
- ²⁴P. Ščajev, S. Miasojedovas, A. Mekys, D. Kuciauskas, K. G. Lynn, S. K. Swain, and K. Jarašiūnas, J. Appl. Phys. **123**, 25704 (2018).
- ²⁵C. H. Swartz, M. Edirisooriya, E. G. LeBlanc, O. C. Noriega, P. A. R. D. Jayathilaka, O. S. Ogedengbe, B. L. Hancock, M. Holtz, T. H. Myers, and K. N. Zaunbrecher, Appl. Phys. Lett. 105, 222107 (2014).
- ²⁶J. Moseley, P. Rale, S. Collin, A. Kanevce, E. Colegrove, J. Duenow, S. Jensen, W. K. Metzger, and M. M. Al-Jassim, 44th IEEE Photovoltaic Specialists Conference, Washington, DC, June 2017.
- ²⁷W. K. Metzger and M. Gloeckler, J. Appl. Phys. **98**, 063701 (2005).
- ²⁸C. R. M. Grovenor, J. Phys. C **18**, 4079 (1985).
- ²⁹L. M. Woods, D. H. Levi, V. Kaydanov, G. Y. Robinson, and R. K. Ahrenkiel, AIP Conf. Proc. 462, 499 (1999).
- ³⁰J. D. Major, Semicond. Sci. Technol. **31**, 093001 (2016).
- ³¹C.-S. Jiang, B. To, S. Glynn, H. Mahabaduge, T. Barnes, and M. M. Al-Jassim, in 2016 IEEE 43rd Photovoltaics Specialists Conference (IEEE, 2016), pp. 3675–3680.
- ³²J. Moseley, P. Rale, S. Collin, E. Colegrove, H. Guthrey, D. Kuciauskas, H. Moutinho, M. Al-Jassim, and W. K. Metzger, "Luminescence Methodology to Determine Grain-boundary, Grain-interior, and Surface Recombination in Thin-Film Solar Cells," J. Appl. Phys. (submitted).
- ³³J. Moseley, W. K. Metzger, H. R. Moutinho, N. Paudel, H. L. Guthrey, Y. Yan, R. K. Ahrenkiel, and M. M. Al-Jassim, J. Appl. Phys. 118, 25702 (2015).
- ³⁴A. Kanevce, J. Moseley, M. Al-Jassim, and W. K. Metzger, IEEE J. Photovoltaics 5, 1722 (2015).
- ³⁵R. K. Ahrenkiel, "Minority carrier lifetime in III-V semiconductors," in Semiconductors and Semimetals (Academic, New York, NY, USA, 1993), Vol. 39, pp. 39–150.
- ³⁶S. A. Jensen, J. M. Burst, J. N. Duenow, H. L. Guthrey, J. Moseley, H. R. Moutinho, S. W. Johnston, A. Kanevce, M. M. Al-Jassim, and W. K. Metzger, Appl. Phys. Lett. **108**, 263903 (2016).
- ³⁷J. Ma, D. Kuciauskas, D. Albin, R. Bhattacharya, M. Reese, T. Barnes, J. V. Li, T. Gessert, and S. Wei, Phys. Rev. Lett. 111, 67402 (2013).
- ³⁸J.-H. Yang, L. Shi, L.-W. Wang, and S.-H. Wei, Sci. Rep. **6**, 21712 (2016).
- ³⁹D. W. Niles, X. Li, P. Sheldon, and H. Höchst, J. Appl. Phys. 77, 4489 (1995).
- ⁴⁰N. M. Terlinden, G. Dingemans, M. C. M. van de Sanden, and W. M. M. Kessels, Appl. Phys. Lett. 96, 112101 (2010).
- ⁴¹N. M. Terlinden, G. Dingemans, V. Vandalon, R. H. E. C. Bosch, and W. M. M. Kessels, J. Appl. Phys. **115**, 33708 (2014).
- ⁴²L. He, J. D. Walker, H. M. Branz, C. T. Rogers, and C. W. Teplin, Appl. Phys. Lett. **101**, 161604 (2012).
- ⁴³D. Kuciauskas, T. H. Myers, T. M. Barnes, S. A. Jensen, and A. M. Allende Motz, Appl. Phys. Lett. 110, 83905 (2017).
- ⁴⁴D. Kuciauskas, D. Lu, S. Grover, G. Xiong, and M. Gloeckler, Appl. Phys. Lett. 111, 233902 (2017).
- ⁴⁵D. K. Simon, P. M. Jordan, T. Mikolajick, and I. Dirnstorfer, ACS Appl. Mater. Interfaces 7, 28215 (2015).
- ⁴⁶G. Lüpke, Surf. Sci. Rep. **35**, 75 (1999).
- ⁴⁷Although PL and SHG intensity varies between grains, the averaged intensities are reproducible when measurement is taken at different areas of the sample. For example, in two DH3 scans in Figs. 5(b) and 5(d), averaged PL intensities are $37.0 \pm 4.1/37.1 \pm 5.4$ and averaged SHG intensities are $14.0 \pm 5.9/12.1 \pm 3.1$.
- ⁴⁸R. E. Treharne, A. Seymour-Pierce, K. Durose, K. Hutchings, S. Roncallo, and D. Lane, J. Phys.: Conf. Ser. 286, 12038 (2011).